Research Article

A new semianalytical method for analysis of the disc-type permanent magnet hysteresis motor in steady-state operational conditions

Ali BEHNIAFAR*, Ahmad DARABI

Department of Electrical & Electronics Engineering, Faculty of Electrical and Robotics Engineering,
Shahrood University of Technology, Shahrood, Iran

Abstract: Considering the characteristics of hysteresis and permanent magnet motors, it seems that these two motors are complements of each other. Thus, their combination yields a motor with an excellent performance. In order to preserve the major advantages of both motors in the new motor, a disc-type slotless structure is chosen. This paper presents a new finite-element method for the modeling of disc-type permanent magnet hysteresis synchronous (PMHS) motor. In this modeling method a new iterative algorithm is used. Programming software has been linked to finite-element software because of its limitation in the modeling of hysteresis phenomena. Validity of the proposed analysis is checked by experimental results. Reasonably close agreement between the two is obtained and good performance of the PMHS motor is verified.

Key words: Hysteresis motor, permanent magnet motor, disc type, modeling, finite element

1. Introduction

Permanent magnet (PM) synchronous motors are good options for small and medium power applications. These motors have several advantages such as high power density (because of the elimination of field winding and usage of high-energy magnets), high torque, high power factor, and high efficiency. However, the major drawback of PM synchronous motors is that they cannot produce starting torque when operated at line frequency. On the other hand, hysteresis motors are usually used in small and very small power and high-speed applications. The stator of these motors is similar to the one in conventional induction motors and their solid rotor has high hysteresis capability. Hysteresis motors have some advantages such as self-starting, low-starting current; high-starting and synchronizing torque; and low noise. However, the disadvantages of these motors are low power factor, high magnetizing current, and low efficiency. Moreover, when a random disturbance happens, the rotor of the hysteresis motor oscillates around the synchronous speed at a low frequency equal to 3–5 Hz. This phenomenon is called "hunting". This happens because the resultant poles of the rotor do not have a specific position on the rotor.

According to the given explanations, it seems that hysteresis and PM motors are complements of each other. Thus, the combination of them causes the disadvantages of the hysteresis motor (or PM motor) to be solved as much as possible.

Perov presented the first PM hysteresis synchronous (PMHS) motor in 1959 [1]. He designed a rotor by combining the permanent magnet and hysteresis materials in a cylindrical structure. The experimental results of this motor showed that the power density was considerably improved. He also indicated that the use of

---

*Correspondence: ali_behniafar@yahoo.com

permanent magnets in the rotor of a hysteresis motor leads to removing many weaknesses of this motor such as low power factor, low efficiency, and hunting. In [2], the effect of a samarium cobalt permanent magnet on the steady-state performance of a cylindrical hysteresis reluctance motor was studied. It was demonstrated that the use of this magnet compared to other magnets like Alnico5 increases the exciting air-gap voltage and thus can improve the machine performance. The implementation of the proposed structure of this reference involves many difficulties because the hysteresis ring is usually built in the foil form. In addition, in this structure the magnets are fixed on nonmagnetic material (aluminum), which causes the magnetic flux to be considerably reduced. Also, in [3], a new structure of cylindrical hysteresis-reluctance motor was investigated in the steady-state condition. This structure has some grooves on the inner surface of the hysteresis ring that cause magnetic saliency. The equations of a cylindrical hysteresis-reluctance motor in the d-q coordinate system were also presented in this reference. Experimental results of this research showed that the hysteresis-reluctance motor has better performance characteristics in comparison to the conventional hysteresis motor. In [4], a cylindrical PMHS motor was investigated, and by using state-space equations, the performance characteristics of this motor were predicted in the time domain. This method in comparison to the previous analytical methods has some advantages such as the capability of prediction of the machine performance characteristics even in the case of having asymmetric or nonlinear parameters. The magnetic equivalent circuit of d-q axes for the mentioned PMHS motor was presented in [5]. In this reference the motor control strategy was also designed. In 2004, a cylindrical PMHS motor by use of the finite-element method (FEM) was analyzed [6] and the Potter and Schmulian model was utilized to predict the rotor hysteresis curve. Some researchers also investigated the PMHS motor, briefly mentioned here due to a lack of direct connection with the subject of this paper: in [7], comparison of the performance of a PMHS motor to other electrical motors in electrical vehicles was performed. The same authors researched in the field of the control of PMHS motors [8,9]. Nasiri et al. [10] and Lesani et al. [11] studied the reduction of speed oscillations (hunting phenomenon) in a PMHS motor and its fast control strategies, respectively. In [12,13], a magnetic equivalent circuit and also an electrical equivalent circuit in the d-q coordinate system were presented for a cylindrical PMHS motor and a control strategy of this motor was investigated.

It should be noted that all the previous studies considered the cylindrical structure of PMHS machines and to date the disc-type PMHS motor has not been investigated. The disc-type structures have prominence compared to the cylindrical structures comprehensively discussed in [14]. One of the prominent features of disc-type structures is the simplicity of their construction schemes in double-sided or multilayer forms that makes them very appropriate for hybrid motors.

This paper introduces the disc-type structure as a new structure for PMHS motors. The the finite-element modeling method is developed to predict the performance characteristics of the proposed motor. Ultimately the validity of this method is verified by the experimental results of a constructed prototype motor.

In the next section, the new structure proposed in this paper is introduced. In Section 3, the finite-element modeling is performed. Finally, the comparison of experimental and simulation results is provided in Section 4.

2. Description of the disc-type PMHS motor

Various structures can be designed and constructed for PMHS motors, but here only the cylindrical structure is considered and investigated. Since disc-type structures have vast variety, the appropriate structure and design algorithm can lead to a high-quality hybrid PMHS motor with proper performance characteristics.

The proposed structure of this paper is similar to the TORUS-type PM motor [14]. This structure includes an inner stator and two outer rotor discs. One of the discs is assembled by magnets that are placed on the holder of ferromagnetic material and the other disc is made of hysteresis material. This structure is illustrated in Figure 1.
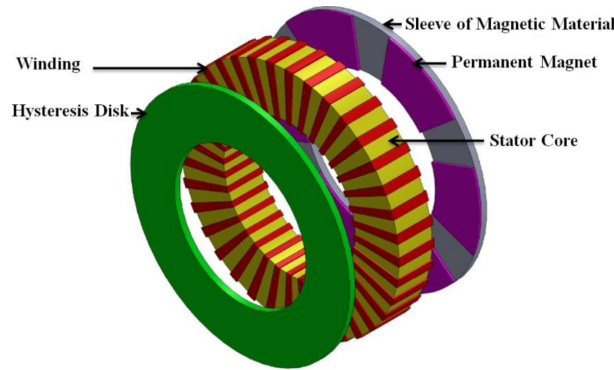
**Figure 1**. Proposed structure of PMHS motor.

In this structure the stator core is nonslotted. Slots on the stator core create some fluctuations in the air-gap flux density (teeth ripple) and as a result the parasitic loss is increased. This consequently reduces the machine efficiency. Moreover, this motor has no pole saliencies because the magnets are magnetized in the axial direction and fixed on the surface of the holder. This feature decreases the torque ripples and the machine acoustic noise. Hence, this motor is highly appropriate for high-speed and high-power applications such as high-power centrifuges. The magnet holder is made of ferromagnetic materials to close the flux path with minimum MMF drop. The magnetic flux in the stator core and the air-gap circulates in the axial direction, while in the hysteresis disc and magnet holder disc it circulates in a circumferential direction. Similar to other axial flux machines, the stator windings of the PMHS motor are in toroidal form.

Now it is useful to briefly present the analytical equations of this motor. These equations can be used for analytical modeling and the design algorithm of the studied motor in steady-state operational conditions. Detailed descriptions are presented in [15].

Since the motor windings are toroidal, the flux linkage of each stator phase is equal to the summation of fluxes in both air-gaps. In other words, the aggregate stator phase voltage is induced by the contributions of both the PM and hysteresis discs. Therefore, it can be concluded that the studied PMHS motor is composed of the series combination of hysteresis and PM motors, and thus its equivalent circuit results from the series combination of their equivalent circuits. Hence, the electrical equivalent circuit of the PMHS motor can be obtained by extracting the equivalent circuit of each of the motors individually and connecting them serially.

The analytical modeling process starts with implementation of Ampere's circuital law. Then, by utilizing Faraday's induction law and flux continuity law, the equivalent circuit of the motors can be obtained. The equivalent circuits of the PM and hysteresis motors are shown in Figure 2. The calculation method for elements of the equivalent circuit of PM motors was presented in several references, such as [16]. The elements of the hysteresis motor circuit are obtained as follows:

$$e_f = -\frac{N_s \, L_e \, t_r \, B_m \, \pi \, \omega_e}{2a} \cos(\omega_e t - \varphi_0), \tag{1}$$
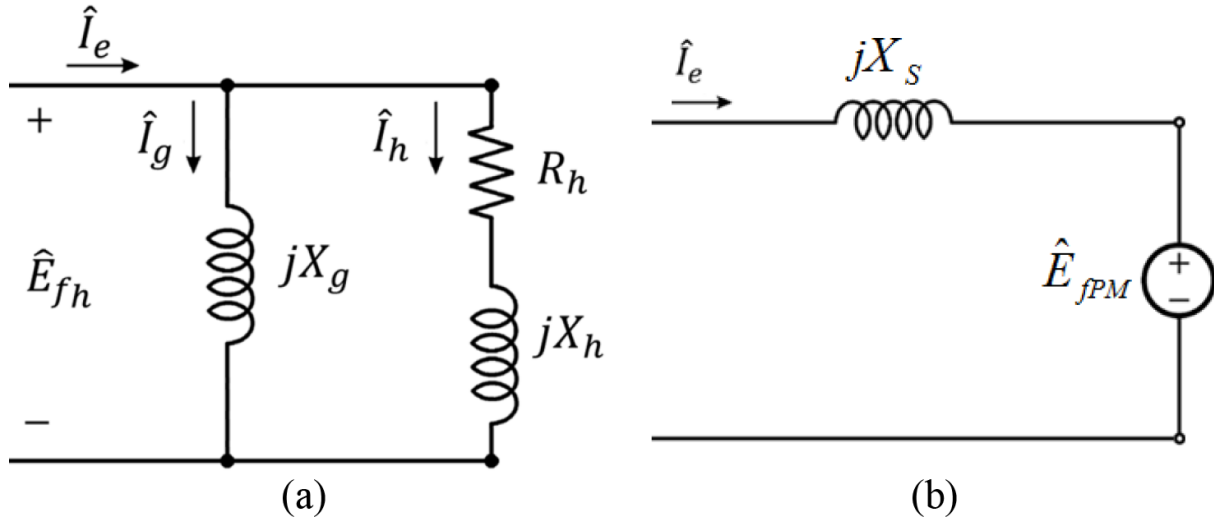
Figure 2. Equivalent circuit per phase obtained from analytical method in steady-state conditions: a) hysteresis motor, b) PM motor.

$$X_g = \frac{1}{K_r} \frac{\left|\hat{E}_f\right|}{\left|\hat{I}_g\right|} = \frac{m\,\mu_0 N_s^2\,L_e\,R_{avg}\,\pi\,\omega_e}{2K_r g\,a^2\,p^2}, \tag{2}$$

$$Z_h = \frac{\hat{E}_f}{\hat{I}_h} = \frac{m\,\mu\,\pi\,\omega_e L_e\,t_r\,N_s^2}{8\,R_{avg}a^2}\angle\frac{\pi}{2} - \alpha = R_h + jX_h, \tag{3}$$

where m, N_s, p, a, L_e, t_r, R_{avg}, and g denote the number of phases, equivalent number of turns of winding by sinusoidal distribution, number of poles, number of parallel current paths per phase, axial length of motor, axial thickness of hysteresis disc, average radius, and air-gap effective length, respectively. Coefficient K_r in Eq. (2) represents the decrease in X_g due to MMF drop in the stator core, which leads to the increment of the motor magnetization current. R_h and X_h are the equivalent impedance of the hysteresis disc.

It is necessary to mention that the distribution patterns of magnetic flux density B_r and field intensity H_r in the hysteresis disc can be formulated based on the elliptical approximation of hysteresis loops, as follows:

$$B_r(t, \varphi_s) = B_m \cos(\omega_e t - \varphi_{se} - \varphi_0), \tag{4}$$

$$H_r(t, \varphi_s) = H_m \cos(\omega_e t - \varphi_{se} - \varphi_0 + \alpha) = \frac{B_m}{\mu}\cos(\omega_e t - \varphi_{se} - \varphi_0 + \alpha), \tag{5}$$

where ϕ_{se}, ϕ_0, B_m, and H_m denote the electrical angle around the stator circumference (with reference to the axis of phase a), initial phase angle, flux density magnitude, and field intensity magnitude, respectively. It should be noted that both magnetic permeability of hysteresis disc μ and hysteresis delay angle α are functions of the amplitude of magnetic field intensity or flux density in the rotor disc.

3. Finite-element modeling of PMHS motor in steady-state operational conditions

In order to increase the accuracy of the performance prediction of the PMHS motor, the FEM has been employed.

The following assumptions are necessary to be adopted during the motor modeling process:

1) The modeling process is performed for steady-state operational conditions in synchronous speed and with maximum loading torque.

2) The magnetic field distributions are assumed uniform in the radial direction (2D analysis).

3) A set of concentric ellipses are utilized as approximate models of the hysteresis loops associated with the rotor disc material.

The analysis of the axial flux machines must be performed on a 3D model but in some cases and conditions we can avoid the time-consuming and complicated 3D analysis method. It is clear that the distribution of magnetic flux density in discs is nonuniform. However, when the discs have low radial and axial thickness, it can be assumed that the distribution of magnetic flux density in discs is uniform with good precision. The experimental results have shown that this approximation is appropriate in the studied motor. Therefore, the 2D model of the motor is used, which is a cross-section of the motor in average radius. Moreover, as outlined in the following sections, it is necessary to use the coupling of finite-element software and programming software to analyze the hysteresis phenomenon in the 2D model. This process itself is time-consuming. The implementation of this process on a 3D model would be very complicated and take a lot of time. This is while the accuracy of calculations increases only slightly.

In analytical modeling of the PMHS motor to calculate induction voltage of total air-gaps $E\wedge_r$ and exciting current $I\wedge_e$ some equations are obtained using Ampere's circuital law and Faraday's induction law and considering some simplifying suppositions.

In order to increase the accuracy of modeling results $E\wedge_r$ and $I\wedge_e$ can be calculated using a finite-element model. In this condition, the equivalent circuit per phase of the PMHS motor in steady-state conditions will be according to Figure 3. In this equivalent circuit, the effects of all components of the stator and rotor such as the winding, stator core, air-gap, hysteresis disc, PMs, and magnet holder in the terminal ports of the motor are included in voltage source $E\wedge_r$ and current $I\wedge_e$.
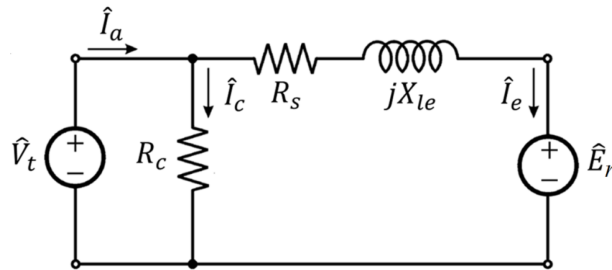
Figure 3. Equivalent circuit per phase of PMHS motor in steady-state conditions.

It should be noted that common finite-element software is not able to identify the operational hysteresis loop corresponding to the terminal voltage of machine. The only ability of such software programs in implementation of a hysteresis loop is that they calculate the magnetic flux density of the machine by inserting exciting current, hysteresis loop characteristics, and the exact position of that loop as inputs (similar to PM implementation). Some finite-element software is able to connect to other software and some provide good environments for programming, so it is possible to meet some specific requirements with this software. Accordingly, in this paper the coupling of COMSOL software with MATLAB software is used. COMSOL is one of the most common finite-element software programs that has high capability in solving finite-element problems and provides

the possibility access all the details. On the other hand, MATLAB has a good programing environment and it skilled at matrix calculations. It should be noted that this time-consuming and complex coupling is unnecessary in the design and analytical modeling of a PMHS motor. The need for accurate numerical analysis and the shortcomings of finite-element software in the right implementation of the hysteresis loops is the main reason for software coupling.

The other significant point is that in this paper a 2D finite-element model is used in order to decrease calculation time. Therefore, all of the flux leakage components of stator windings are considered in the finite-element model and do not appear in Figure 3, except leakage reactance of end winding X_{le}.

R_C and R_s represent the equivalent resistance per phase of stator core loss and resistance per phase of stator windings, respectively. The calculation methods for these parameters can be found in several references, such as [17,18].

In the equivalent circuit of Figure 3, exciting current $I\wedge_e$ and air-gap voltage $E\wedge_r$ are functions of hysteresis characteristics of the rotor disc (μ and α), while $E\wedge_r$ is dependent on $I\wedge_e$. Considering that hysteresis characteristics are dependent on the terminal voltage, $I\wedge_e$ and $E\wedge_r$ will become functions of terminal voltage. Due to the lack of simple analytical equations to describe these functions, iterative methods should be used to relate $I\wedge_e$ and $E\wedge_r$ to terminal voltage. On the other hand, unlike the analytical method, in finite-element modeling for each optional hysteresis loop there is no possibility of calculation of $I\wedge_e$ and $E\wedge_r$ by mathematic equations. Therefore, in order to solve this problem, another iterative algorithm is needed.

The proposed algorithm of this paper for finite-element modeling of the PMHS motor in the steady state is represented in Figure 4. In the beginning of this algorithm, for an input voltage V_{in}, an initial hysteresis loop is selected. Therefore, maximum magnetic field intensity H_m will be determined. Then distribution of the circumferential component of magnetization in the hysteresis disc is calculated by using this loop. The formulations of the magnetization distribution were discussed in [15] and due to page limitations the presentation is ignored here. By supposing the maximum torque for the PM disc, back-EMF angle δ_{PM} and PM rotor position are obtained. Then an initial exciting current is selected. By applying the distribution of magnetization and the exciting current to the finite-element model, the maximum value of the circumferential component of magnetic field intensity $H_{m,FEM}$ is achieved. If the relative difference between $H_{m,FEM}$ and H_m is acceptable, the selected exciting current is true; otherwise, the exciting current must be changed. After the correct current is obtained, the fundamental wave of linkage flux is calculated by the finite-element model and thus the air-gap voltage corresponding to the selected loop is calculated. Then, by supposing the exciting current as the reference phasor, the terminal voltage V_t will be calculated. If the relative difference between V_{in} and V_t is acceptable, the selected hysteresis loop is true; if not, the hysteresis loop must be changed.

4. Experimental results for a prototype PMHS motor

In this section the validity of the proposed finite-element model is checked by experimenting on a prototype motor and comparing the results. Therefore, a prototype 150-W PMHS motor is designed and constructed, whose characteristic parameters are listed in the Table. The hysteresis disc of this motor is made of Fe-Cr-Ni-Mo-C alloy. The hysteresis loops of this material after a particular annealing process are obtained and the elliptical approximation characteristics of them are shown in Figure 5.

The manufactured PMHS motor of this paper is of the two-layer type. It has two hysteresis discs, two stators, and a double-sided PM disc, which is placed between the two stators. Figure 6 illustrates the separate components of the motor as well as the test stand. It should be noted that the simulation of the whole motor structure would be very time-consuming. Thus, it is essential to use the symmetry rules. If the manufactured
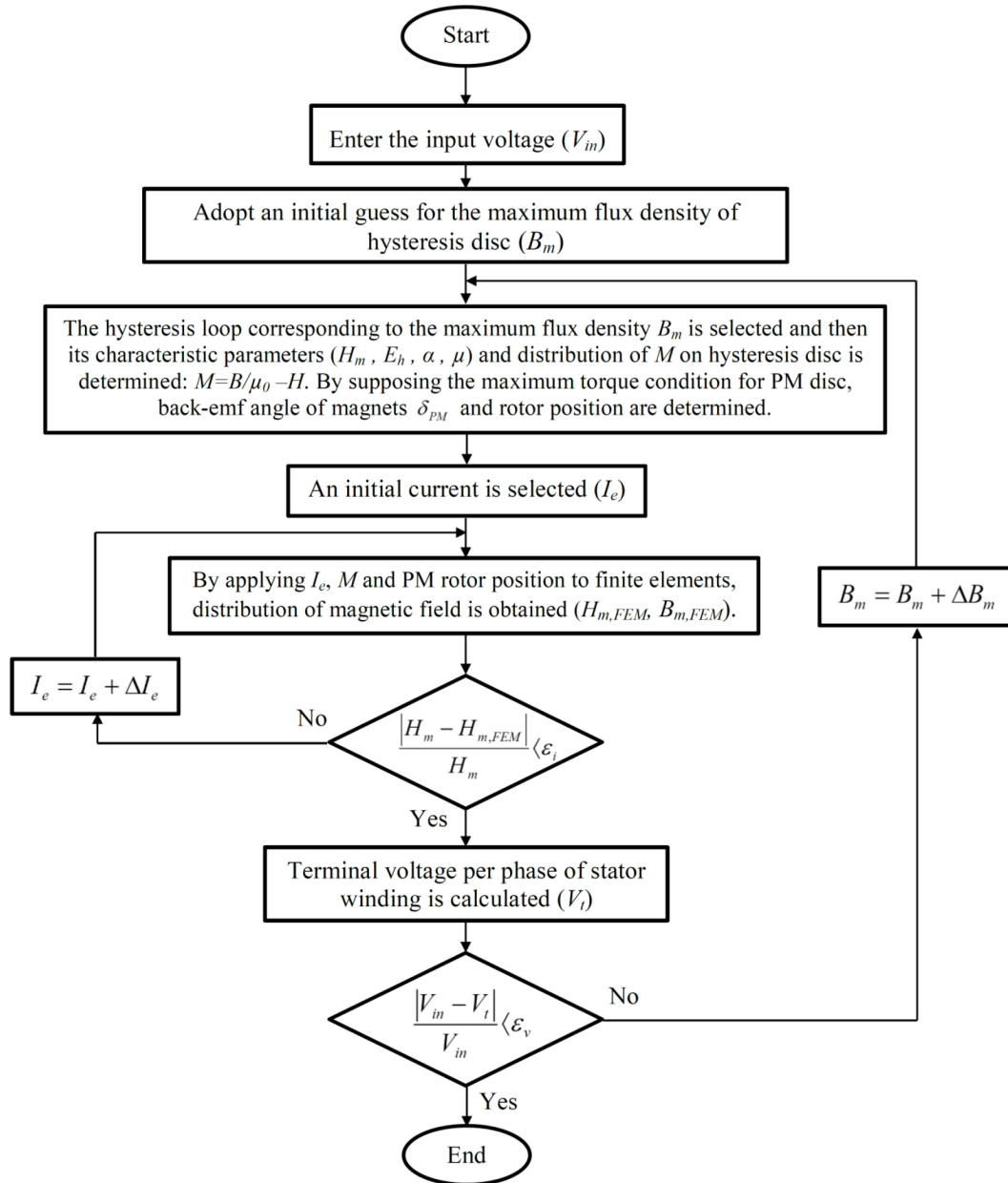
Start

Enter the input voltage (V_{in})

Adopt an initial guess for the maximum flux density of hysteresis disc (B_m)

The hysteresis loop corresponding to the maximum flux density B_m is selected and then its characteristic parameters (H_m, E_h, α, μ) and distribution of M on hysteresis disc is determined: $M=B/\mu_0 - H$. By supposing the maximum torque condition for PM disc, back-emf angle of magnets δ_{PM} and rotor position are determined.

An initial current is selected (I_e)

By applying I_e, M and PM rotor position to finite elements, distribution of magnetic field is obtained ($H_{m,FEM}$, $B_{m,FEM}$).

$B_m = B_m + \Delta B_m$

$I_e = I_e + \Delta I_e$

No

$\dfrac{\left|H_m - H_{m,FEM}\right|}{H_m} \langle \varepsilon_i$

Yes

Terminal voltage per phase of stator winding is calculated (V_t)

No

$\dfrac{\left|V_{in} - V_t\right|}{V_{in}} \langle \varepsilon_v$

Yes

End

Figure 4. The proposed algorithm of this paper for finite-element modeling of PMHS motor in steady state.

motor (Figure 6) is cut from the middle of the PM disc, the two halves are exactly identical, so, by applying the symmetrical criteria, it is not necessary at all to simulate the whole motor, which would be very time-consuming. Hence, in the previous sections, one side of this motor is investigated.

Figure 7 shows the operational elliptical hysteresis loops resulting from finite-element modeling of the studied PMHS motor for various values of terminal voltage. It is demonstrated that the variations of the terminal voltage not only change the loop area but also change the loop width and its direction angle. This is due to the variations of the hysteresis delay angle and magnetic permeability of the hysteresis disc.

The most significant operational characteristics of the prototype motor resulting from the finite-element modeling process and experimental tests are presented in the remainder of this section. The simulation results

**Table.** Design Information of the studied PMHS motor.

Value	Quantity
3	Number of phases
50 Hz	Nominal frequency
12 V	Nominal input phase voltage
150 W	Nominal input 3-phase power
4	Number of poles
4	Number of coils per phase
28	Number of winding turns per coil
25.5 mm	Inner radius
45 mm	Outer radius
3 mm	Thickness of hysteresis disc
2 mm	Axial thickness of PMs
2 mm	Width of PMs
3 mm	Width of magnet holder disc
3.2 mm	Air-gap length
19 mm	Thickness of stator yoke
Y	Connection type of stator windings
One-layer lap winding	Winding type
Complete	Winding pitch

are drawn for input phase voltages between 2 and 14 V. Due to some limitations such as the maximum current limit and loss of synchronism (because of friction), the motor could not be tested over the entire mentioned range of terminal voltage. It should be noted that the loading conditions are better in the PMHS motor due to the increase of synchronous torque and this is one of the reasons for the suitability of the mentioned combination.

The variation of the input current with respect to the variation of the terminal voltage is illustrated in Figure 8. Figure 9 displays the dependency of the input power factor on the terminal voltage. As shown in this Figure, as the field intensity rises, the hysteresis angle and relative permeability of the hysteresis disc first increase and then decrease. It makes the power factor have the same trend, too. The operational range of the studied motor is located in descending part. Unfortunately, the copper loss of this motor is somewhat high, keeping the power factor unaltered with increasing input voltage. The little variation seen in the graph of the power factor can be interpreted due to the measurement.

Moreover, the variation of the three-phase input power versus the terminal voltage is presented in Figure 10 and the curve of the stator copper loss is plotted in Figure 11. In Figure 12 the variation of the electromagnetic torque versus terminal voltage is graphed. In this Figure, two separate components of electromagnetic torque resulting from finite-element modeling are shown, which are hysteresis torque and PM torque, which have been compared to experimental torque. It is observable that hysteresis torque is much less than PM torque. The material used for fabricating the hysteresis disc (considering our limitations in choosing good material) is producing torque that is enough for synchronizing and oscillation damping of motor. Moreover, if the purpose of combining these motors is to optimize the performance of the hysteresis motor, this result would be valuable because the major disadvantages of the hysteresis motor (such as low synchronous torque, low power factor, and low efficiency) are obviated.
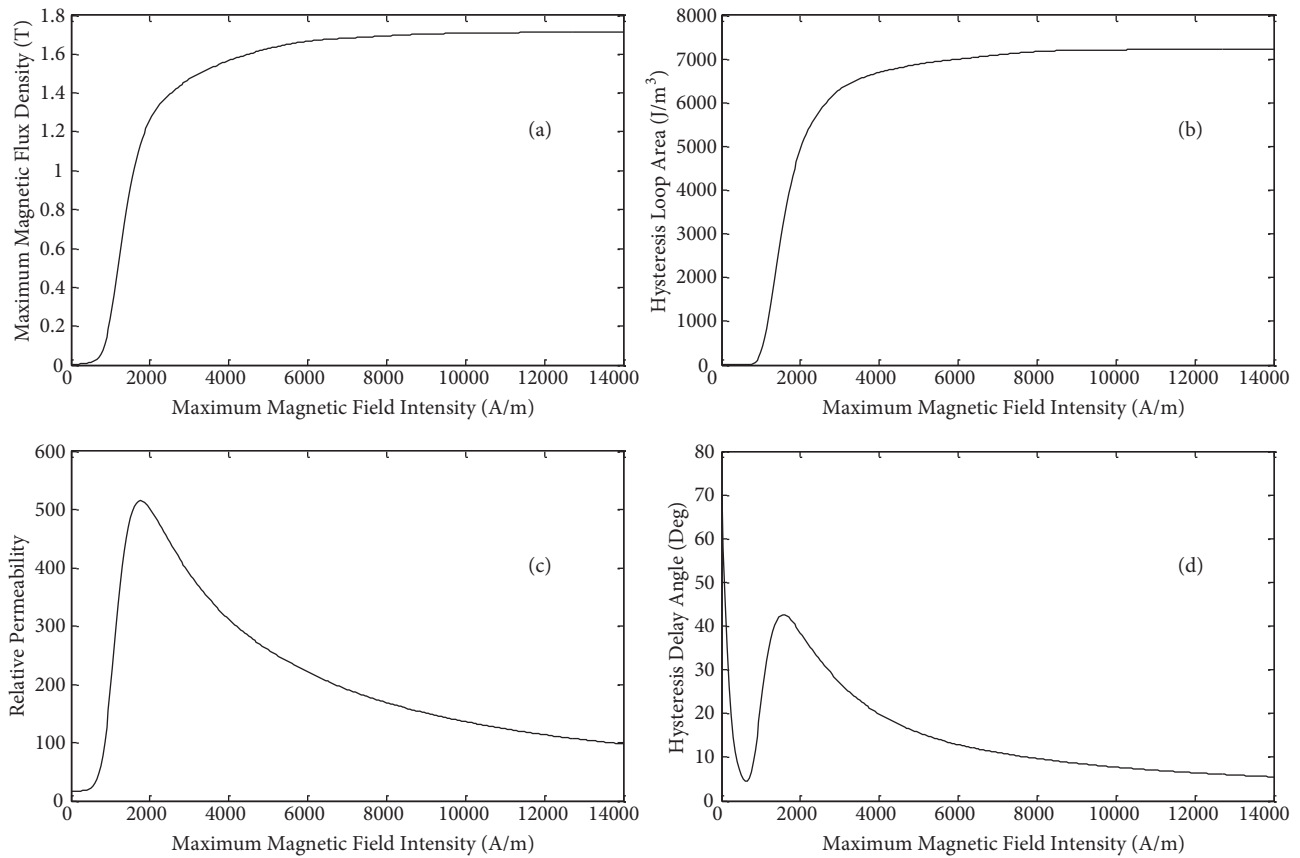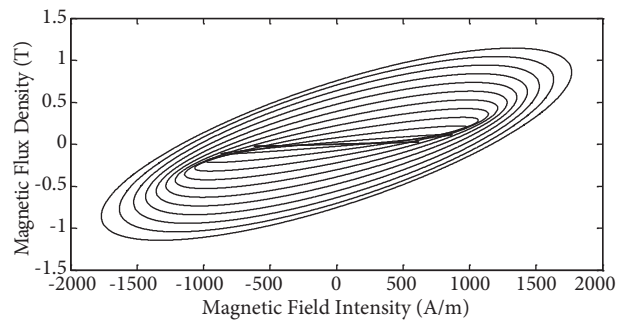
Figure 5. Elliptical approximation characteristics of the hysteresis disc material in the studied motor versus magnetic field intensity amplitude of the loop: a) magnetic flux density of the loop, b) area of the loop, c) relative permeability, and d) hysteresis delay angle.


**Figure 6**. Various components of the test stand of the PMHS motor.

**Figure 7**. Operational elliptical hysteresis loops resulting from the finite-element modeling of the PMHS motor for various terminal voltages.

It is obvious from the results that by increasing the input voltage of the motor, the input current, electrical power, and losses will all be increased, too. This occurs due to the increase in the area of the motor operational hysteresis loop that is valid for all types of hysteresis and PMHS motors.
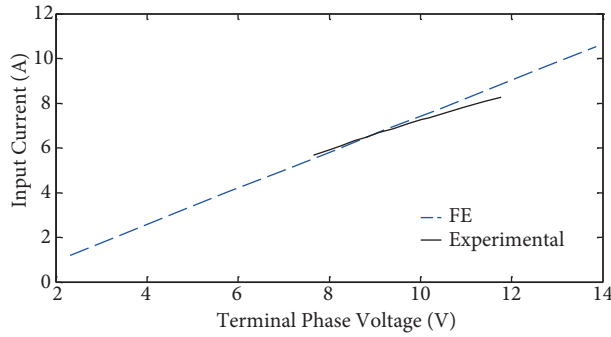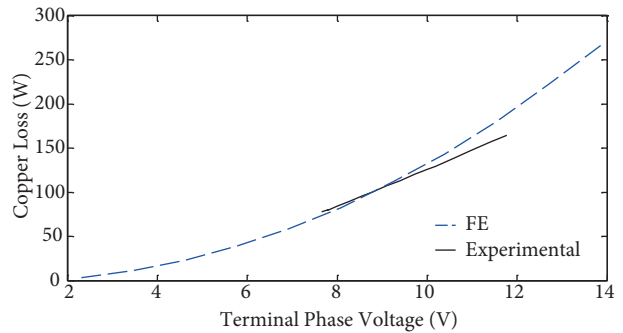
Figure 8. Variation of input current versus terminal voltage.
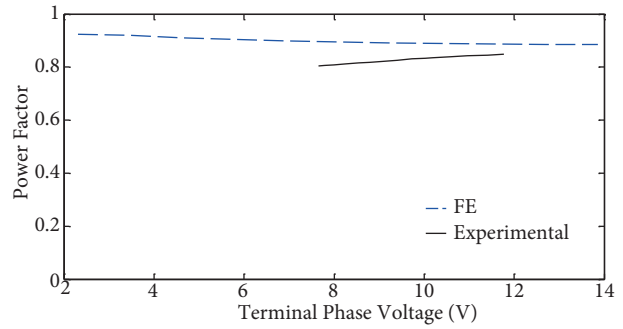
Figure 9. Variation of power factor versus terminal voltage.
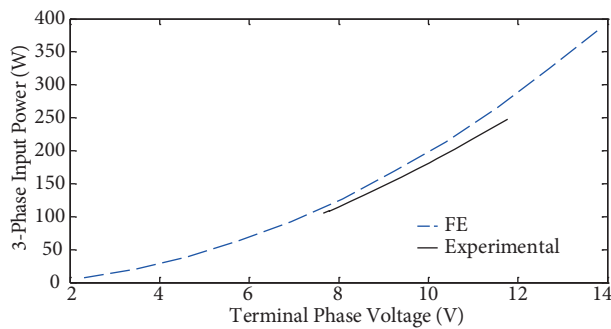
Figure 10. Variation of 3-phase input power versus terminal voltage.

Figure 11. Variation of 3-phase copper loss versus terminal voltage.

It is observable from the above Figures that the finite-element and experimental results are very close to each other with an excellent approximation. As mentioned before, the main reason for their difference is that the finite-element model belongs to the maximum loading condition while this condition cannot easily be implemented in experimental tests. However, in this work, it is attempted to achieve the maximum loading conditions in experiments as much as possible.

Now it is appropriate to investigate the results of the finite-element model in line voltage of 12 V (current equals 7.8 A). For creating mesh, first, a mesh for half of a slot pitch is introduced and then this mesh is repeated for the remaining components. The meshing process is shown in Figure 13. It is evident from this Figure that the stator core has triangle elements and other components have rectangular elements. Distributions of magnetic flux density and magnetic flux lines are shown in Figure 14.

5. Conclusion

The hysteresis and PM motors individually have unique features and it seems that they are complements of each other. Thus, the combination of these motors can lead to a motor with excellent performance characteristics. In this paper, a hybrid PMHS motor is introduced with a new structure. This structure holds the prominent features of both the hysteresis motor (e.g., low noise and starting current levels) and the PM motor in the resulting PMHS motor. Moreover, the major weaknesses of the hysteresis motor such as the hunting effect, low efficiency, low power factor, and low output torque are also obviated in the presented PMHS motor. Also in this paper, a new finite-element model for the PMHS motor in steady-state conditions with maximum loading is
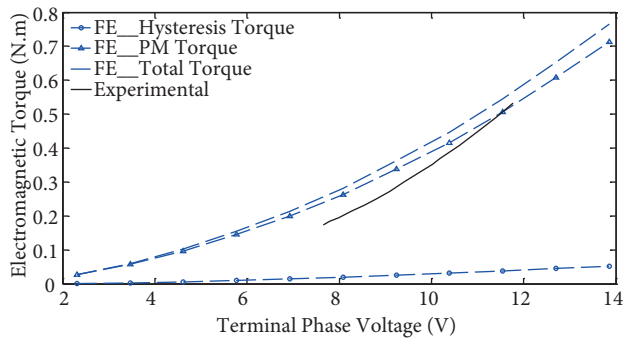
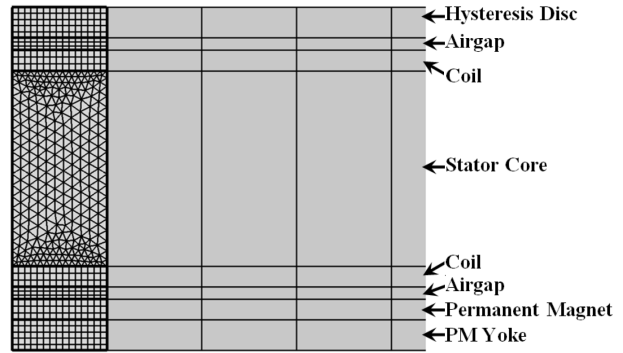**Figure 12**. Variation of electromagnetic torque versus terminal voltage.

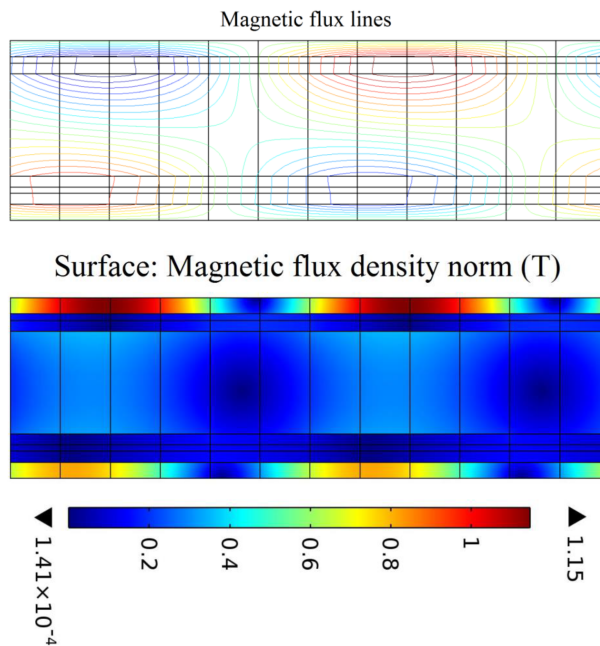**Figure 13**. Mesh created on half of a slot pitch.

Figure 14. Distribution of magnetic flux density and magnetic flux lines.

presented. In order to implement this modeling method, a new iterative algorithm is introduced. Furthermore, for making possible the comparison and validation of this numerical modeling method, a prototype PMHS motor has been designed, fabricated, and tested. The results have good agreement and verify the validity of the theoretical prediction method and also confirm the good performance of the disc-type PMHS motor.

References

[1] Wakui G. Hysteresis motor with reaction torque and its analysis. Electr Eng Jpn 1978; 98: 58-67.

[2] Rahman M, Osheiba A, Little T. Effects of samarium cobalt permanent magnet on the performance of polyphase hysteresis-reluctance motors. IEEE T Magn 1984; 20: 1765-1767.

[3] Rahman M, Osheiba A. Steady-state performance analysis of polyphase hysteresis-reluctance motors. IEEE T Ind Appl 1985; 21: 659-663.

[4] Rahman M, Qin R. Starting and synchronization of permanent magnet hysteresis motors. IEEE T Ind Appl 1996; 32: 1183-1189.

[5] Qin R, Rahman M. Magnetic equivalent circuit of PM hysteresis synchronous motor. IEEE T Magn 2003; 39: 2998-3000.

[6] Kurihara K, Rahman M. Transient performance analysis for permanent-magnet hysteresis synchronous motor. IEEE T Ind Appl 2004; 40: 135-142.

[7] Rahman M, Qin R. A permanent magnet hysteresis hybrid synchronous motor for electric vehicles. IEEE T Ind Electron 1997; 44: 46-53.

[8] Qin R, Rahman M. DSP based torque and speed controls of the permanent magnet hysteresis synchronous motor. In: IEEE 1997 Electric Machines and Drives Conference; 18–21 May 1997; Milwaukee, WI, USA. New York, NY, USA: IEEE. pp. 9.1-9.3.

[9] Qian J, Rahman M. Analysis of field oriented control for permanent magnet hysteresis synchronous motors. IEEE T Ind Appl 1993; 29: 1156-1163.

[10] Nasiri-Gheidari Z, Lesani H, Tootoonchian F. A new hunting control method for permanent magnet hysteresis motors. Iranian Journal of Electrical & Electronic Engineering 2006; 2: 121-130.

[11] Lesani H, Darabi A, Nasiri-Gheidari Z, Tootoonchian F. Very fast field oriented control for permanent magnet hysteresis synchronous motor. Iranian Journal of Electrical & Electronic Engineering 2006; 2: 34-40.

[12] Rabbi S, Rahman M. Equivalent circuit modelling of a hysteresis interior permanent magnet motor for electric submersible pump. IEEE T Magn 2016; 52: 1-4.

[13] Rabbi S, Halloran M, LeDrew T, Matchem A, Rahman M. Modelling and V/F control of a hysteresis interior permanent magnet motor. IEEE T Ind Appl 2016; 52: 1891-1901.

[14] Hatami H, Bannae-Sharifian M, Feyzi M. A new method for improved design of low speed axial flux permanent magnet machines used in HEV. Tabriz Journal of Electrical Engineering 2015; 45: 51-64 (in Persian with an abstract in English).

[15] Behniafar A, Darabi A. Analytical modelling of disc type permanent magnet hysteresis motor in steady state conditions. In: PSC 31st International Power System Conference; 24–26 October 2016; Tehran, Iran. pp. 1-9 (in Persian with an abstract in English).

[16] Zhu Z. The electromagnetic performance of brushless permanent magnet DC motors - with particular reference to noise and vibration. PhD, University of Sheffield, Sheffield, UK, 1991.

[17] Pyrhonen J, Jokinen T, Hrabovcova V. Design of Rotating Electrical Machines. 2nd ed. New York, NY, USA: Wiley, 2014.

[18] Gieras J. Permanent Magnet Motor Technology: Design and Applications. 3rd ed. Boca Raton, FL, USA: CRC Press, 2010.